Escola de Primavera de Transição e Turbulência
Blumenau 2022

ABCM
13th Spring School on Transition and Turbulence
September 19th-23rd, 2022, Blumenau, SC, Brazil

EPTT-2022-0017
COMPARISON OF DIFFERENT MODELING STRATEGIES FOR THE PREDICTION OF LIFT AND DRAG OF AN UAV WING

Breno Lopes Tumelero
Filipe Dutra da Silva
Federal University of Santa Catarina - Campus Joinville, Dona Francisca St., 8300, Joinville, SC – Brasil
breno.tumelero@teg.ufsc.br
filipe.dutra@teg.ufsc.br

Rafael Gigena Cuenca
Federal University of Santa Catarina - Campus Joinville, Dona Francisca St., 8300, Joinville, SC – Brasil
rafael.cuenca@ufsc.br

Abstract. *An accurate detection of stall on a wing is fundamental to define several parameters in aircraft design, such as lift-off speed, required runway length and maximum take-off weight. When using computational fluid dynamics tools, the correct numerical modeling is a key factor to guarantee the accuracy of the predictions of lift and drag coefficients. The present study proposes a simulation model, based on the open-source code OpenFOAM, to predict the lift and drag coefficients of wings with low-to-moderate aspect ratios at low Reynolds number. Incompressible Reynolds Averaged Navier Stokes simulations were performed for a wing with aspect ratio of 4, based on the Wortmann FX 63-137 airfoil, at a Reynolds number of 100k. Validation was performed through comparisons with experimental data and sensitivity tests to the size of the computational domain and to turbulence inflow parameters are provided. Also, grid dependency tests were conducted based on the Grid Convergence Index. In order to assess the influence of turbulence modeling on the results, two models were considered: k-ω SST and the Spalart-Allmaras. Finally, the polars are generated for each case, and the variations in the absolute values of CL and CD for each model were assessed, as well as the influence of the modeling in the detection of the wing stall. The proposed model was able to provide accurate results with relatively low computational cost, being suitable for the design of low-speed, unmanned-aircraft wings.*

Keywords: *unmanned aerial vehicle, aerodynamic parameters, OpenFOAM*

1. INTRODUCTION

The preliminary design phase is a key point in the aeronautical industry, as important concepts and different project philosophies can be tested and validated, leading to an optimal final aircraft. As an example, choices made during this phase for a SAE aerodesign competition project may completely change the aircraft characteristics, regarding both aerodynamic and performance. Thereby, a high-lift approach would result in a smaller, high load wing, sacrificing the plane's efficiency, where a flying wing, based on a reflex airfoil, would have increased wing area and efficiency, at the cost of higher complexity and take-off speed.

Aiming to reduce the development cost and time, modern computational fluid dynamics (CFD) came up as an important tool to allow quick data evaluation, removing the need of building a prototype during the early project stages. With the help of such tools, different wing configurations, airfoils and more complex geometries can be modeled and simulated on a given condition within a day's time. Furthermore, CFD can be taken to a bigger scenario, working as an accurate design tool for different situations, such as wingtip devices for an UAV, wing-fuselage interaction and stall detection.

Said so, this study aims to validate a simulation model using the open source code OpenFOAM for the assessment of the aerodynamic characteristics of UAV wings. The aim is to obtain a model to correctly predict the aerodynamic forces and stall point, for use in both preliminary design and final development phases. In order to reach this objective, sensitivity analyses to the size of the domain, turbulence modeling and inlet turbulence parameters were performed, and finally, validation is conducted by comparisons with experimental data.

2. METHODOLOGY

This section elucidates the theory and steps needed for the numerical simulation setup and tests performed in order to improve the accuracy of the model.

2.1 Geometry

At first, as a way to attest the accuracy of the results, a geometry with available experimental data was adopted. Thus, the case chosen for validation was an Wortmann FX 63-137 wing, with aspect ratio (AR) of 4, shown in Fig. 1. The

aerodynamic coefficients were obtained by Bastedo and Mueller (1986) and Ananda *et al.* (2012) through wind tunnel tests at a Reynolds number of 10^5. Both tunnels presented turbulent intensity levels below 0.1%.

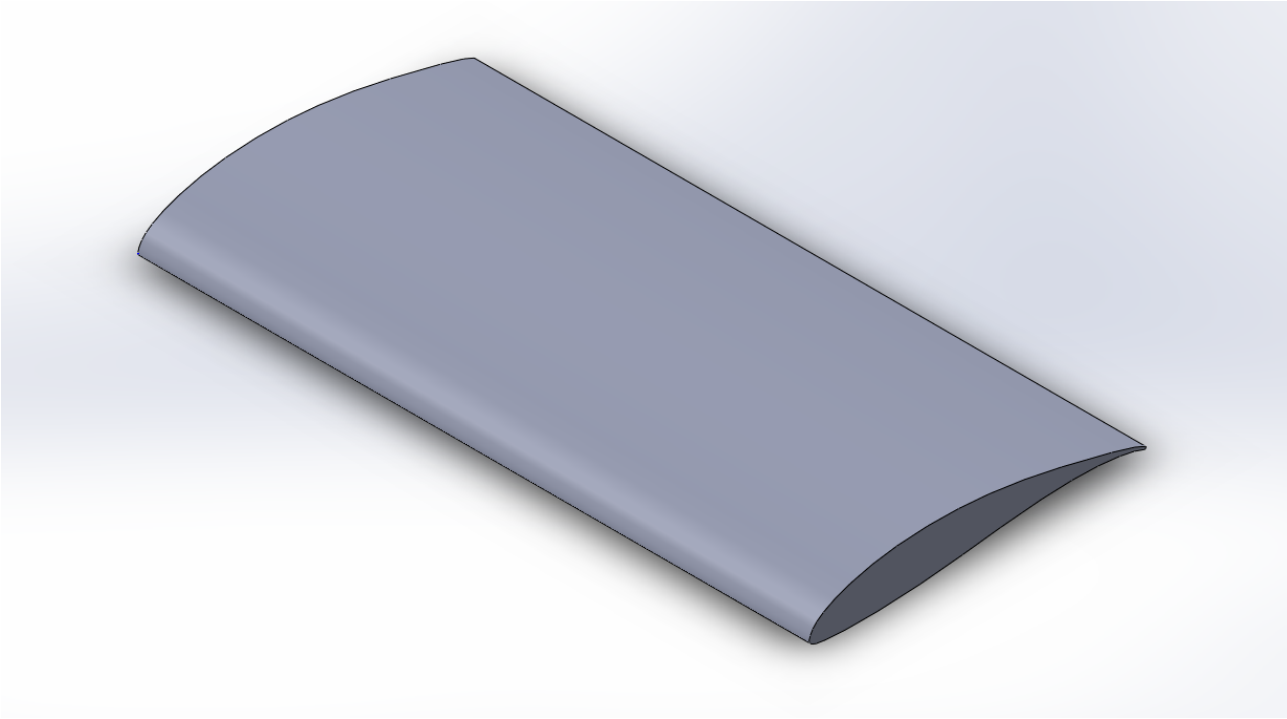

Figure 1. AR 4 Wortmann FX 63-137 wing.

The first experimental data was obtained by Bastedo and Mueller (1986) using a wind tunnel located at the Notre Dame Aerospace Laboratory (Fig. 2), having a 24 in.^{2} cross section, and using a 6-in chord wing model. This way, the estimated gap between the wingtip and the tunnel wall was around 9 in.

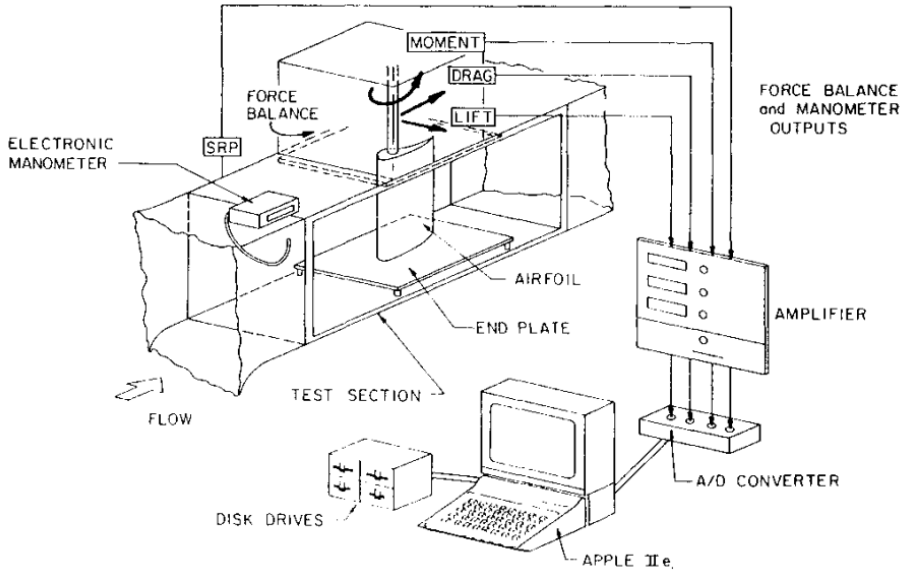

Figure 2. Notre Dame Aerospace Laboratory wind tunnel experiment setup, Bastedo and Mueller (1986)

As for the second case, data was acquired by Ananda *et al.* (2012) using the UIUC low-speed subsonic wind tunnel, which has a 2.8 x 4 ft cross-section, and although no test wing model dimensions were provided, Fig. 3 shows a greater clearance. In this picture, the mirror sting was used for interference tests only, and was not in the final experiment.

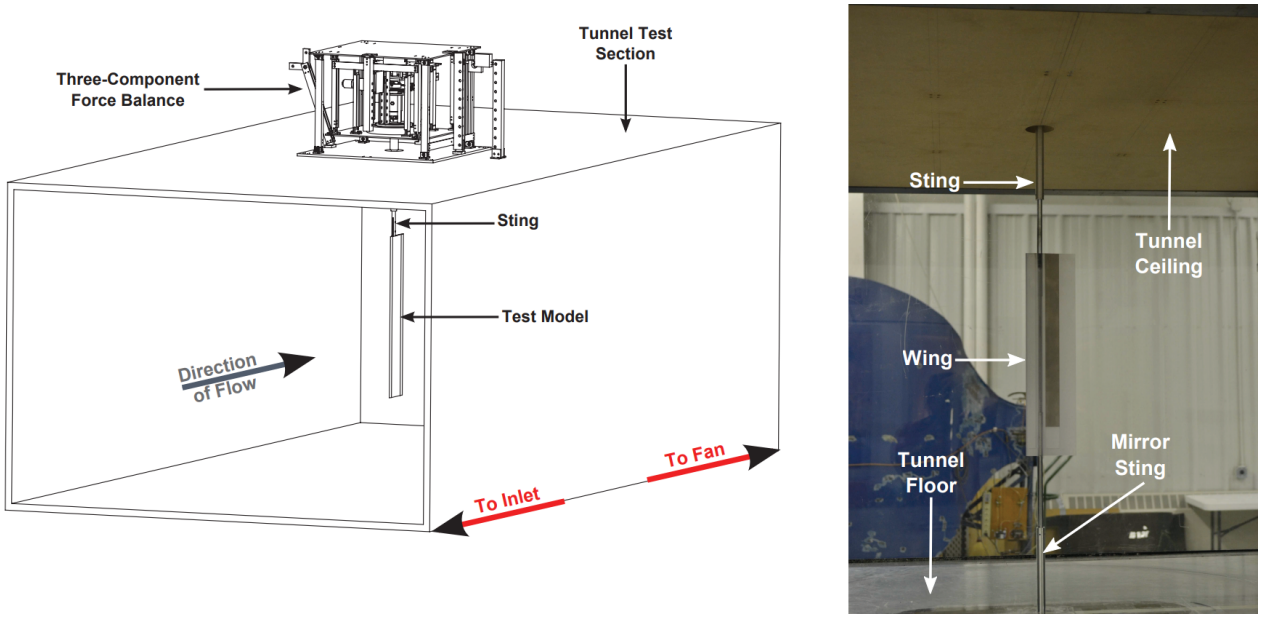

Figure 3. UIUC low-speed subsonic wind tunnel experiment setup, Ananda *et al.* (2012)

This way, to match the required Reynolds number, as seen in Eq.1, the wing was modeled with a 1 m semispan and 0.5 m chord (C), resulting in a freestream velocity V of around 3 m/s. Lastly, standard air value was used for the kinematic viscosity $\nu = 1.5x10^{-5}$ m^2/s.

$$Re = \frac{V \cdot C}{\nu} \tag{1}$$

2.2 Simulation model

The simulations were performed using the OpenFOAM v8 code (Greenshields, 2020), whereas the computational mesh was generated on Salome 9.7. The mesh was composed mainly by tetrahedra, with layers of prismatic cells near the wing surface to discretize the boundary layer gradients, as shown in Fig.4.

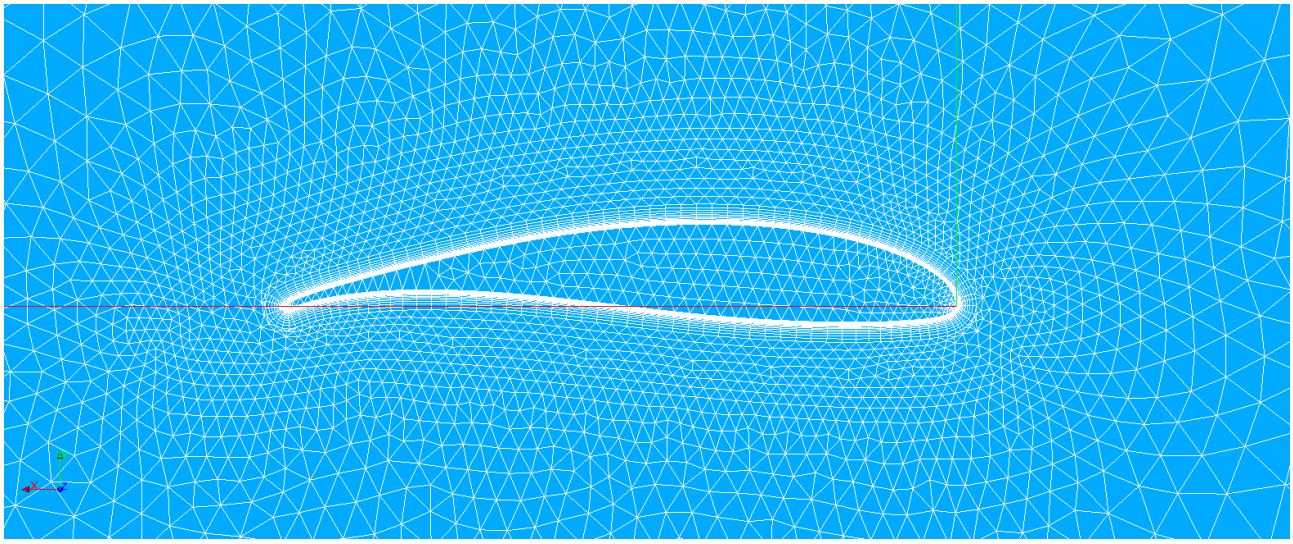

Figure 4. Mesh around the wing.

Also on the wing surface, a structured triangular mesh was generated, as depicted in Fig.5. This approach allowed a faster mesh generation with better quality , also facilitating the meshing process on corners and highly curved regions, such as the leading and trailing edge.

To ensure the reliability of the results, several grid related tests were made, starting with the domain size sensibility test. The baseline domain is hexahedron-shaped, with length and height of a hundred wing chords,and width of ten times the wing semispan. The base domain is shown in Fig.6. The second tested domain was obtained by doubling the width,

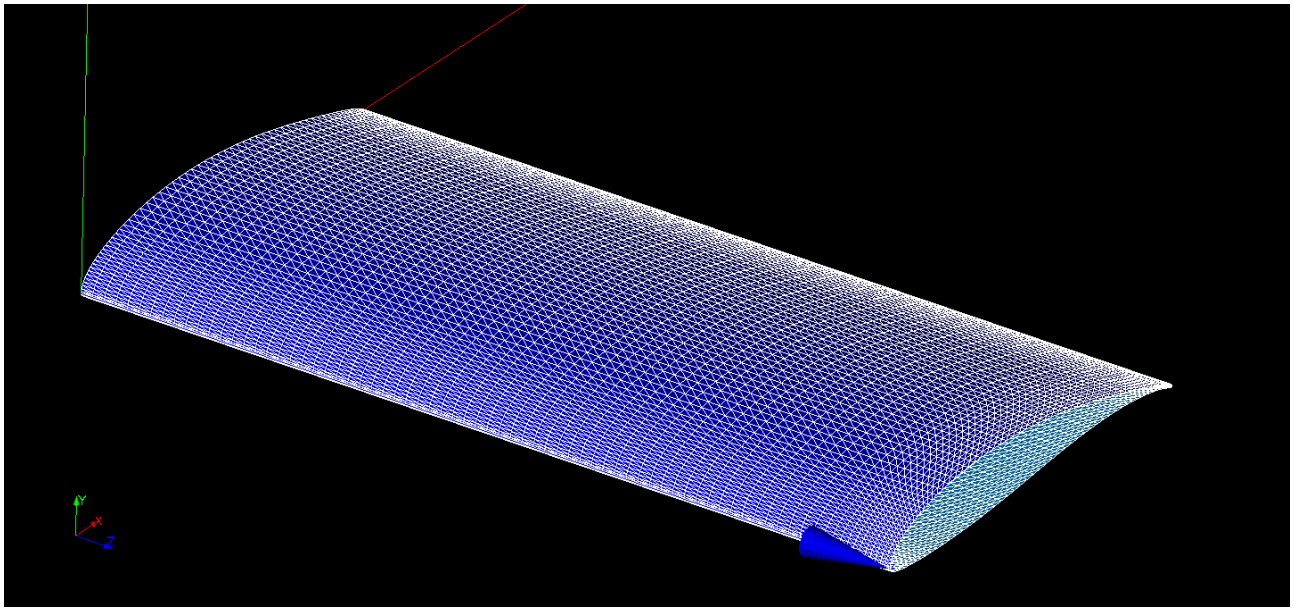

Figure 5. Mesh on the wing surface.

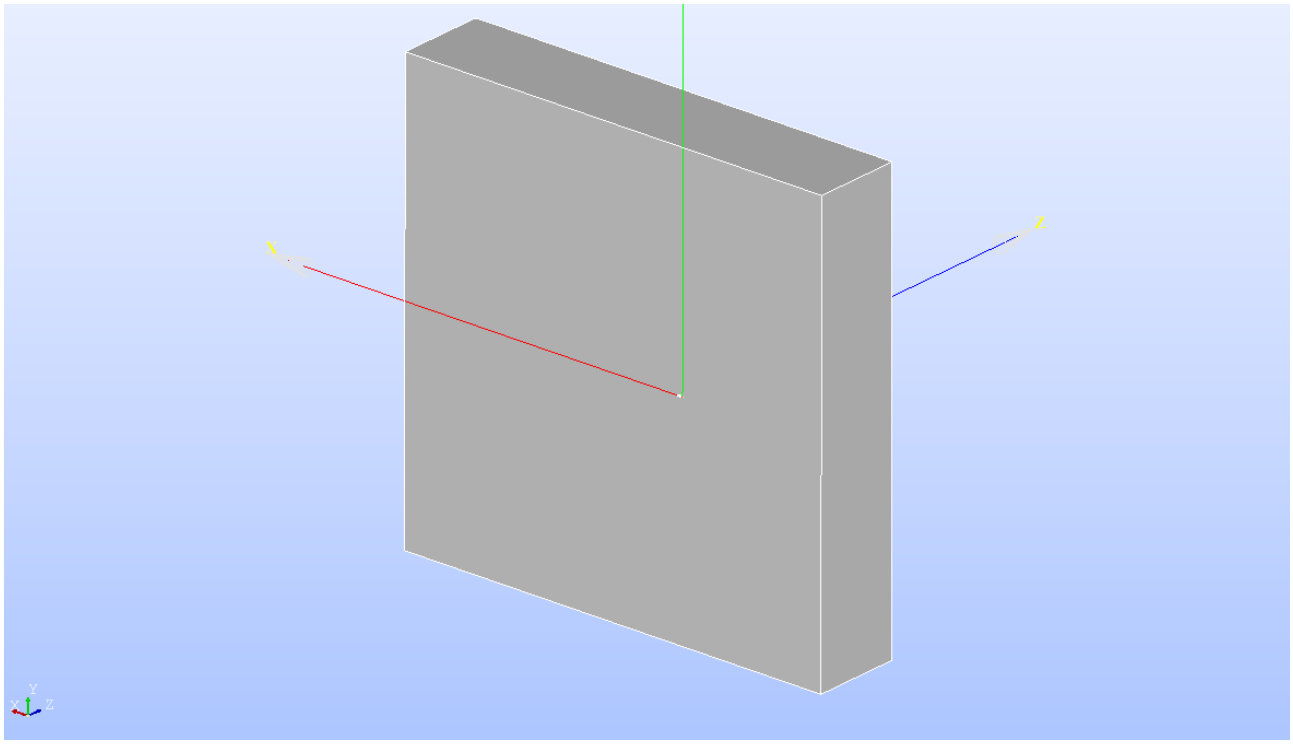

Figure 6. Geometry of the domain.

and the third one by halving the height and length of the baseline domain. Only in this test, simulations were performed at an angle of attack equal to $12°$.

Furthermore, sensitivity tests to grid refinement were performed using the Grid Convergence Index method (GCI), described by Roache (1997) and Celik *et al.* (2008), which estimates how close the mesh is to reaching an asymptotic value by increasing its refinement. The initial cell sizes were defined according to previous researches (Tumelero *et al.*, 2021), and the refinement ratio r used was the minimum recommended value of 1.3, as shown in Eq.2-3, where N is the total cells number and V_i is the cell volume (Celik *et al.*, 2008).

$$r = \frac{h_{coarse}}{h_{fine}} \tag{2}$$

$$h = \left[\frac{1}{N}\sum_{i=1}^{N} V_i\right]^{1/3} \tag{3}$$

After defining a baseline medium mesh (2), a coarser mesh (1) and a finer mesh (3) were built using the mentioned refinement ratio and the lift and drag coefficients (CL and CD) were selected as variables to be analyzed (ϕ). Next, using the difference between the variable values $\epsilon_{12} = \phi_1 - \phi_2$, the apparent method order p can be calculated according to Eq.4.

$$p = \frac{1}{ln(r)} ln\left|\epsilon_{12}/\epsilon_{23}\right| \tag{4}$$

Then, with the above being calculated, the extrapolated values from the finer mesh, the relative error and the extrapolated relative error can be obtained through Eq.5-7.

$$\phi_{ext}^{23} = \frac{(r_{23})^p \phi_3 - \phi_2}{(r_{23})^p - 1} \tag{5}$$

$$e_a^{23} = \frac{\phi_3 - \phi_2}{\phi_3} \tag{6}$$

$$e_{ext}^{23} = \frac{\phi_{ext}^{23} - \phi_3}{\phi_{ext}^{23}} \tag{7}$$

Lastly, the GCI for each mesh combination is calculated using a safety factor of 1.25 (Eq.8), which results in a reliability of 95%, showing how close the results of the current mesh is to the point where an increase in refinement does not affect the obtained values anymore (Wilcox, 1993).

$$GCI = \frac{1.25 e_a}{(r^p) - 1} \tag{8}$$

As for the interpolation schemes, it the second-order limitedLinear scheme was used for turbulence variables to reduce numerical diffusion as mush as is possible. Moreover, the second-order linearUpwind was used for velocity, as it improved convergence and stability.

Reynolds-Averaged Navier-Stokes (RANS) were performed, as it can provide steady state data with different turbulence models, each one with its own advantage, while having a way lower computational cost when compared to time-depedent simulations. This being said, two turbulence models were chosen for the simulations: the Spalart-Allmaras and the k-ω SST.

The Spalart-Allmaras model was developed for the usage in the aerospace industry, and uses a single equation to solve the modified turbulent viscosity ratio (Langley, 2022), hence being very cost efficient, but underpredicting flow separation, which may lead to an overpredicted maximum CL.

On the other hand, k-ω SST (Menter, 1994) need two equations: one for the turbulence kinetic energy k, and the second for the specific dissipation rate ω. Although it has a slightly higher computational cost, this model is known for its good accuracy in predicting the separation point, thus having good stall prediction capabilities.

For the inlet turbulence parameters, a comparison was made between generic standard CFD values for turbulent intensity (I) and eddy viscosity ratio (μ_t/μ) and recommended values for wing aerodynamics usage according to Spalart and Rumsey (2007), as shown in Eq.9-10 and Tab.1. Here, U is the reference freestream velocity, c is the reference chord length, and resulting I and μ_t/μ values are be calculated through Eq.11-12 (Università di Genova, 2021).

Table 1. I and μ_t/μ values used during the simulations.

Case	I	μ_t/μ
1	1%	5
2	0.08165%	0.02

These parameters affect profile drag, and may also change transition and stall point, being extremely important for both cruise flight and take-off performance.

$$k = 1 \times 10^{-6} U^2 \tag{9}$$

$$\omega = \frac{5U}{c} \tag{10}$$

$$I = \frac{\sqrt{\frac{2}{3}k}}{U} \tag{11}$$

$$\frac{\mu_t}{\mu} = \frac{k}{\nu \cdot \omega} \tag{12}$$

It is important to mention that all the simulations for the grid refinement tests were performed using the k-ω SST turbulence model, along with the suggested turbulence inlet values.

3. RESULTS

This section presents the outcomes from the tests and analyses described previously, including graphics and numerical data.

3.1 Domain size sensibility test

The domain size tests showed that the baseline domain presented results close to the larger ones, as can be seen in Tab.2. So the baseline domain initially set is already large enough for the intended accuracy. Due to the very small difference in the absolute coefficients and the cell count, no reduction in size or further changes had to be made.

Table 2. Domain size sensibility test results.

Domain	CL	CD	Cell count
Baseline	1.15469	0.159658	1356347
Double width	1.15905	0.160321	1377671
Half height/length	1.15737	0.160311	1354546

3.2 Grid convergence test

As mentioned earlier, the grid refinement was chosen using the GCI method, where the wing was simulated at an angle of attack of 16°, a critical operation point for being close to the stall start, one of the key characteristics intended for the final analysis. For this, three different meshes shown in Tab.3 were used, all of them with a y+ value below 1, according to the required condition for correctly solving the boundary layer.

The main idea behind this test is to check how far the base mesh is from reaching the same value as an infinitely refined mesh, and if the difference is too much to be overlooked, a higher cell count mesh, also with a higher computational cost may be considered.

Table 3. GCI test meshes.

Mesh	Cell count	r	CL	CD
Coarse	603058	1.3102	1.34959	0.228989
Baseline	1356347	-	1.2971	0.216235
Refined	3084173	1.3150	1.29608	0.214794

Then, the GCI is obtained according to the steps explained in section 2.2, as can be seen in Tab.4, which shows that the baseline mesh has good precision when compared to the predicted extrapolated coefficients.

Although the refined mesh shows results slightly closer to the asymptotic value, it present a significant increase of simulation time relative to the baseline mesh. So, in case of high accuracy drag evaluations, a more refined mesh may be better suited for the case, as the apparent method order for the CD is smaller than for the CL.

3.3 Turbulence inlet parameters

To guarantee the simulation model performs as close as possible to the real case, two different value pairs for k and ω were selected to show the importance of a correct initial boundary condition setup. The first pair, resulted in a turbulent intensity of 1% and an eddy viscosity ratio of 5, commonly standard values found on CFD solvers, while the second uses the Eq.9 and 10, resulting in a turbulent intensity of 0.08165% and an eddy viscosity ratio of 0.02.

Table 4. GCI test results.

Parameter	Value
p(CL)	15.02041467
p(CD)	8.310993249
$\phi_{ext}(CL)$	1.296059786
$\phi_{ext}(CD)$	0.214610452
$e_a^{23}(CL)$	-0.0787%
$e_a^{23}(CD)$	-0.6709%
$e_{ext}^{23}(CL)$	-0.0016%
$e_{ext}^{23}(CD)$	-0.0855%
$e_{ext}^{2ext}(CL)$	-0.0803%
$e_{ext}^{2ext}(CD)$	-0.7570%
$GCI_{23}(CL)$	0.0019%
$GCI_{23}(CD)$	0.1068%
$GCI_{2ext}(CL)$	0.0020%
$GCI_{2ext}(CD)$	0.1205%

The wing is then simulated at an angle of attack (alpha) range from 0 to 20°, as illustrated in Fig.7 and 8. Results show that a higher turbulent intensity may slightly increase drag, especially at lower angles, but also slows flow separation at the wing upper surface, leading to a smaller lift decrease after stall, underpredicting it. On the other hand, lower values (such as the ones found in high quality wind tunnels) present higher CL and lower drag values, but also a more abrupt stall, leading to a quick lift reduction.

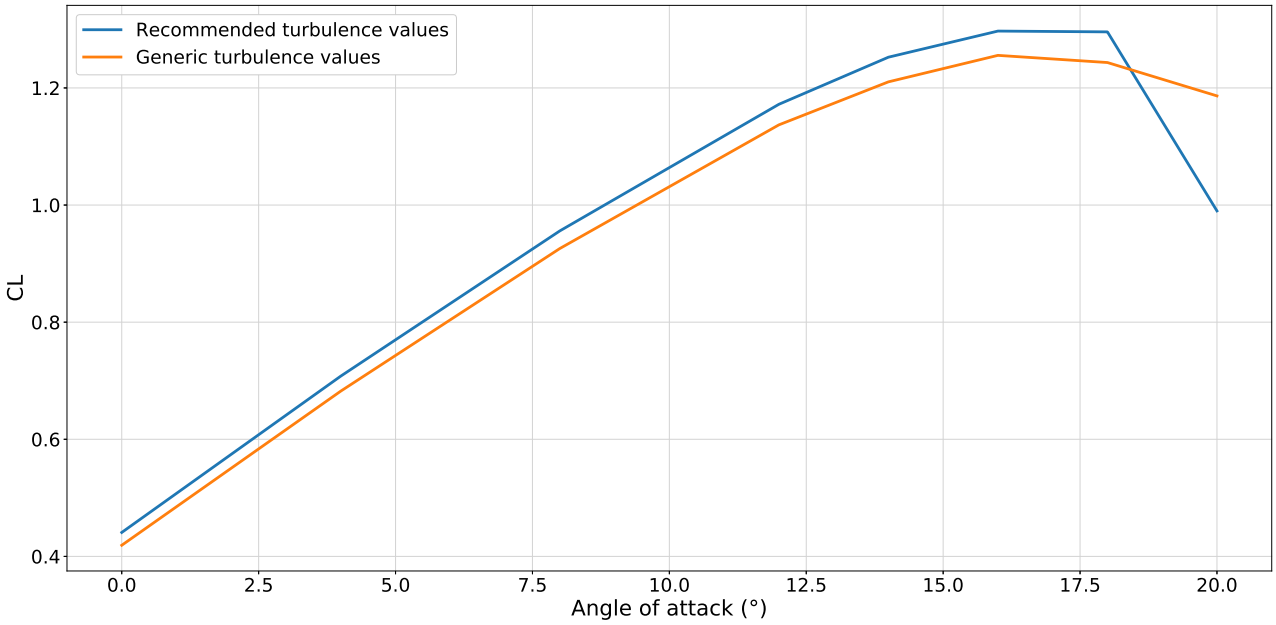

Figure 7. CL x alpha curve for both turbulence parameters.

3.4 Turbulence model

After the recommended turbulence parameters were chosen for the final evaluation, using the same alpha range as the previous test, the obtained CL and CD data from both turbulence models were compared to the polars from Ananda *et al.* (2012) and Bastedo and Mueller (1986), allowing to point some important aspects for each polar (Fig.9 and 10).

While the k-ω SST model is able to predict reasonably well the stall point, the lift curve slope is a bit smaller than the other ones near the stall point. Also, the shift between the curves may be related to the different geometry modeling approaches, such as semispan or full sized wing, domain/wind tunnel section size, etc.

Also, the Spalart-Allmaras model proved to be extremely effective, matching the Ananda *et al.* (2012) polar almost entirely, and still being one of the most computational efficient RANS models available. However, it fails to predict the correct stall point, a previously mentioned expectation.

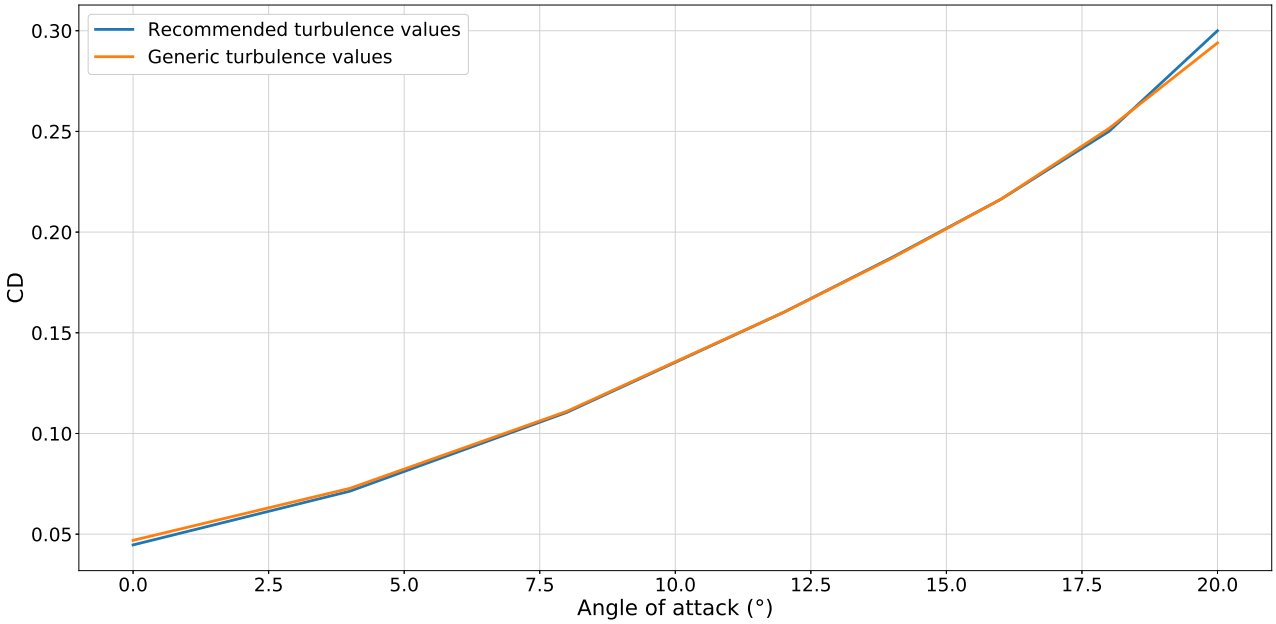

Figure 8. CD x alpha curve for both turbulence parameters.

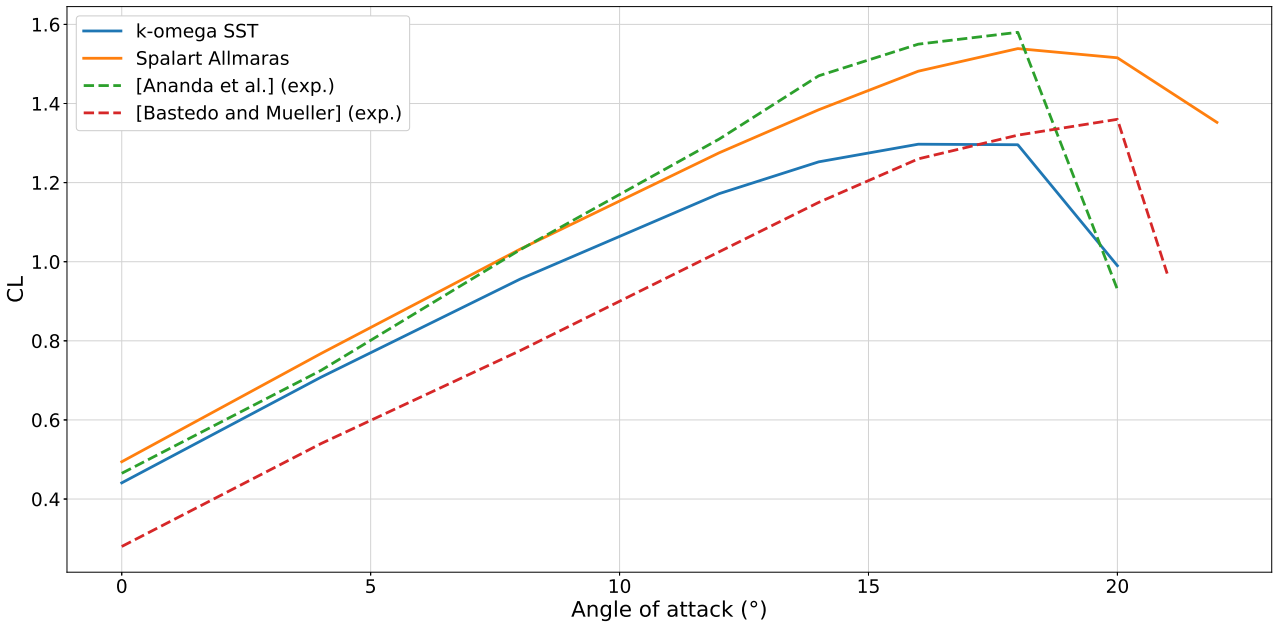

Figure 9. CL x alpha curve for both turbulence models.

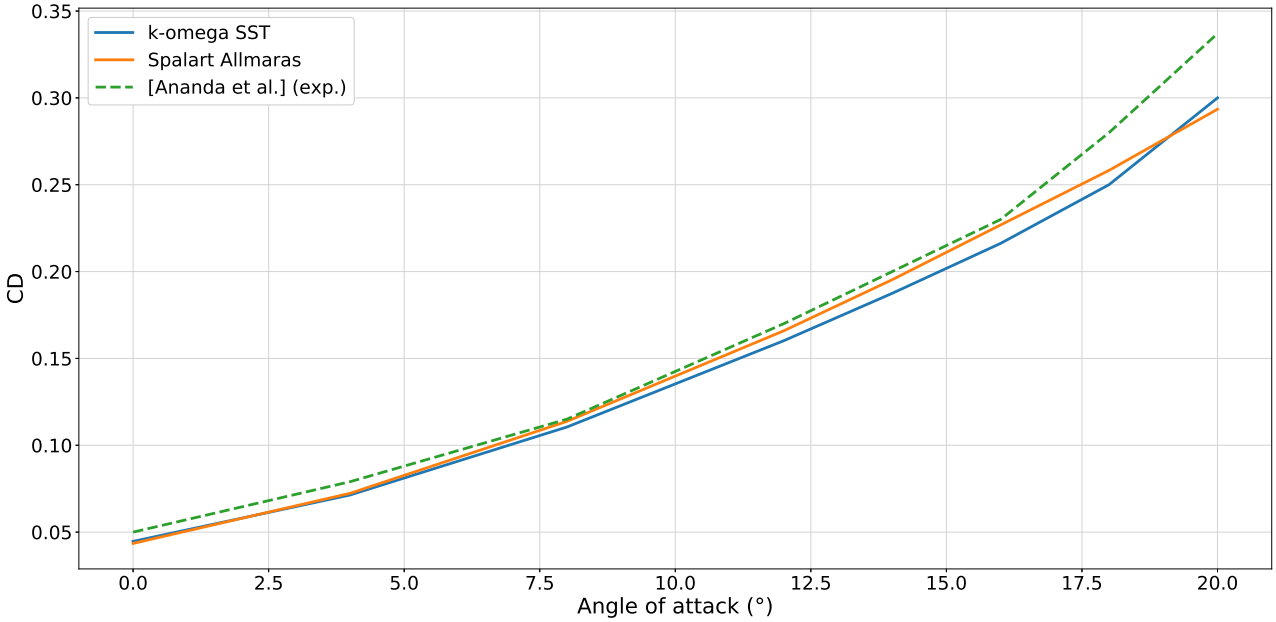

Figure 10. CD x alpha curve for both turbulence models.

4. CONCLUSIONS

The present study successfully validated a numerical simulation model for low speed wings, including the domain size, mesh refinement, inlet parameters and turbulence models.

About the turbulence models, the Spalart-Allmaras proved to be extremely attractive for both its low computational cost and good agreement with experimental data, as soon as the stall detection is not an interest point. Now the k-ω SST model, although showing a small mismatch at high alpha values, is still a viable choice for correctly predicting the stall and having good computational cost and accuracy.

In future studies, it is intended to add to the analysis the Langtry-Menter SST turbulence model, also known as the k-kl-ω, due to its transitional capabilities.

5. ACKNOWLEDGEMENTS

The authors of this paper would like to thank the Naval Simulation Laboratory (LaSiN-UFSC) for granting access to the workstation used for running the numerical simulations performed during this research. The authors would also like to thank PROEX - Pró Reitoria de Extensão (UFSC) for all the support given to the NISUS aerodesign team.

6. REFERENCES

Ananda, G., Sukumar, P. and Selig, M., 2012. "Low-to-moderate aspect ratio wings tested at low reynolds numbers". ISBN 978-1-62410-185-4. doi:10.2514/6.2012-3026.

Bastedo, W.G. and Mueller, T.J., 1986. "Spanwise variation of laminar separation bubbles on wings at low reynolds number". *Journal of Aircraft*, Vol. 23, No. 9, pp. 687–694. doi:10.2514/3.45363.

Celik, I., Ghia, U., Roache, P., Freitas, C., Coloman, H. and Raad, P., 2008. "Procedure of estimation and reporting of uncertainty due to discretization in cfd applications". *J. Fluids Eng.*, Vol. 130, p. 078001. doi:10.1115/1.2960953.

Greenshields, C., 2020. *OpenFOAM v8 User Guide*. The OpenFOAM Foundation, London, UK. URL <https://doc.cfd.direct/openfoam/user-guide-v8>.

Langley, N., 2022. "Spalart-allmaras model". Langley Research Center. URL <https://turbmodels.larc.nasa.gov/spalart.html>.

Menter, F.R., 1994. "Two-equation eddy-viscosity turbulence models for engineering applications". *AIAA Journal*, Vol. 32, No. 8, pp. 1598–1605. doi:10.2514/3.12149.

Roache, P.J., 1997. "Quantification of uncertainty in computational fluid dynamics". *Annual Review of Fluid Mechanics*, Vol. 29, No. 1, pp. 123–160. doi:10.1146/annurev.fluid.29.1.123.

Spalart, P. and Rumsey, C., 2007. "Effective inflow conditions for turbulence models in aerodynamic calculations". *Aiaa Journal - AIAA J*, Vol. 45, pp. 2544–2553. doi:10.2514/1.29373.

Tumelero, B., Costa, S., Silva, L. and Dutra da Silva, F., 2021. "Estudo de metodologia para dimensionamento de endplates em aeronaves de baixas velocidades". doi:10.26678/ABCM.CREEM2020.CRE2020-0124.

Università di Genova, 2021. "Turbulence and cfd models: Theory and applications - dicca". URL <http://www3.dicca.unige.it/guerrero/turbulence2020/slides/6closure_models_RANS_part3.pdf>.

Wilcox, D.C., 1993. *Turbulence modelling for CFD*. DCW Industries, La Cañada.

7. RESPONSIBILITY NOTICE

The authors are the only responsible for the printed material included in this paper.